Contents lists available at ScienceDirect

Acta Materialia

journal homepage: www.elsevier.com/locate/actamat

Full length article

Concurrent strengthening of ultrafine-grained age-hardenable Al-Mg alloy by means of high-pressure torsion and spinodal decomposition

Yongpeng Tang [a], Wataru Goto [a, 1], Shoichi Hirosawa [a, *], Zenji Horita [b], Seungwon Lee [c], Kenji Matsuda [c], Daisuke Terada [d]

[a] Department of Mechanical Engineering and Materials Science, Yokohama National University, 79-5 Tokiwadai, Hodogaya-ku, Yokohama 240-8501, Japan
[b] Department of Materials Science and Engineering, Kyushu University, Fukuoka 819-0395, Japan
[c] Graduate School of Science and Engineering, University of Toyama, Toyama 930-8555, Japan
[d] Department of Mechanical Science and Engineering, Chiba Institute of Technology, Narashino 275-0016, Japan

ABSTRACT

In this study, the age-hardening behavior and precipitate microstructures of severely-deformed and then artificially-aged Al-13.4 wt%Mg alloy has been investigated by Vickers hardness test, X-ray diffraction (XRD) analysis, transmission electron microscopy (TEM) and atom probe tomography (APT). The combined processing of high-pressure torsion (HPT) and aging treatment at a temperature below spinodal lines results in a higher attained hardness of ~HV296 with an age-hardenability (i.e ΔHV31 ± 2) comparable to that of the undeformed specimen without HPT (i.e. ΔHV33 ± 2). The corresponding TEM microstructures consist of modulated structures associated with spinodal decomposition, and quantitative estimation of the amplitude, as well as the wavelength, of Mg fluctuations was successfully conducted by APT for the first time for this alloy system. The linear relationship between the increment of Vickers hardness and the estimated amplitude of the undeformed specimen supposed that Kato's spinodal-hardening mechanism works even in the HPTed specimen with a high number density of grain boundaries. Therefore, our proposed strategy; i.e. taking advantage of spinodal decomposition, is regarded as a convincing approach to achieving concurrent strengthening by ultrafine-grained and precipitation hardenings for the alloys that decompose via spinodal decomposition.

© 2017 Acta Materialia Inc. Published by Elsevier Ltd. All rights reserved.

1. Introduction

Among strengthening mechanisms of aluminum alloys, both of precipitation hardening and hardening by grain refinement are primarily important, and thus many efforts have been done for achieving concurrent strengthening by the two strengthening mechanisms [1–9]. Severe plastic deformation (SPD) such as equal-channel angular pressing (ECAP), accumulative roll bonding (ARB) and high-pressure torsion (HPT) is now a well-established method to obtain ultrafine grains at submicrometer or nanometer scale [10], but the induced hardening by the ultrafine grains (i.e. ultrafine-grained hardening) is often diminished or spoiled by the subsequent aging treatment because preferential precipitation at dislocations and grain boundaries becomes predominant in place of

refined transgranular precipitates [4,6,11]. However, the authors recently reported that the hardness of the HPTed specimen of 2091Al-Li-Cu alloy can be further increased to > HV290 by means of aging treatment at temperatures below spinodal lines within the metastable α-Al + δ'-Al$_3$Li field of Al-Li binary system [6,9]. From the results of in-situ small-angle X-ray scattering (SAXS) measurement, their proposed strategy of "taking advantage of spinodal decomposition" was considered to be applicable not only to the Al-Li-Cu alloy but also to other alloys that decompose via spinodal decomposition; e.g. highly concentrated Al-Mg alloys.

Although there exists different terminology regarding how to indicate the formed zones or phases [12], the phase decomposition sequence of Al-Mg alloys with high Mg concentrations can be written after Sato et al. [13,14] and Dauger et al. [15–17];
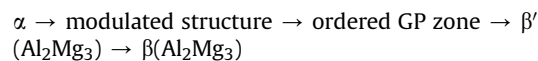
$\alpha \rightarrow$ modulated structure $\rightarrow$ ordered GP zone $\rightarrow \beta'$ (Al$_2$Mg$_3$) $\rightarrow \beta$(Al$_2$Mg$_3$)

---

where α is the original supersaturated solid solution, GP zone stands for a L1$_2$-type ordered structure with a stoichiometric composition of Al$_3$Mg (also indicated as β″), β′ is the semicoherent hexagonal intermediate phase and β is the equilibrium phase with a complex face-centered cubic (fcc) structure. Modulated structure associated with spinodal decomposition is initially formed, and then GP zones are developed in relationship to the modulations, if aged at a temperature below spinodal lines within the metastable α-Al + Al$_3$Mg field of Al-Mg binary system [13]. Such modulated structure can be observed along the [001]$_α$ direction by transmission electron microscopy (TEM) [13−16] and small-angle neutron scattering (SANS) [17], but quantitative estimation of the amplitude of Mg fluctuations has never succeeded, unlike in the case of the wavelength, due to the drawbacks of their transmission imaging and reciprocal space techniques (For example, overlapping of multi-wavelength developing toward different directions cannot be avoided on TEM observation, whereas the smearing effect of large wavelength bears many uncertainties about compositional evaluation by SANS).

In this study, therefore, an age-hardenable Al-13.4 wt%Mg (Al-14.7 at%Mg) alloy subject to HPT and low-temperature aging has been investigated as a model alloy to verify the effectiveness of our proposed strategy to achieve concurrent strengthening; i.e. "taking advantage of spinodal decomposition". The amplitude as well as the wavelength of modulated structures was successfully quantified by atom probe tomography (APT) for the first time, and then correlated to the increment in Vickers hardness through a spinodal-hardening mechanism proposed by Kato et al. [18]. By taking into account the fact that the wavelength is sufficiently smaller than average size of ultrafine grains, spinodal decomposition is supposed to proceed even in the HPTed specimen with a high number density of grain boundaries.

2. Experimental

In this study, an Al-13.4 wt%Mg (Al-14.7 at%Mg) cast ingot with impurity Cu, Fe, Mn and Zn less than 0.01 wt% has been utilized as a model alloy after homogenization treatment at 718 K for 1210 ks, followed by water quenching. Both of 10 mm square pieces and 10 mmφ disks with 1 mm thick were taken from the ingot by electrical discharge machining. All the specimens were solution-treated at 723 K for 3.6ks and then water quenched in order to obtain the super-saturated solid solutions (Note that the maximum solubility of Mg in Al is 18.6 at% at 723 K [19]). HPT was performed at room temperature within 3.6ks after quenching under an applied pressure of 6 GPa for 5 revolutions (See the details in Ref. [5]). Aging treatment was subsequently conducted on the square pieces of the undeformed specimen without HPT as well as the disks of the HPTed specimen at a temperature below the spinodal line (e.g. 343 K [13]) for various times.

The age-hardenability of those specimens was investigated by a microhardness tester (Matsuzawa MMT-X1) with a load of 4.9N for a dwelling time of 15s. The hardness of each specimen was determined as an average value of five tested points out of seven ones with an accuracy of ±HV2. X-ray diffraction (XRD) analysis was conducted for both the specimens in the "before aging" condition by a X-ray analytical instrumentation (Rigaku RINT-2000) using Cu-Kα radiation (wavelength λ = 0.15418 nm) at 40 kV and 200 mA. The foils for TEM observation were prepared by the electrolytic twin-jet polishing technique with 15 vol% nitric acid in 85 vol% methanol at ~253 K. TEM microstructures and the corresponding selected-area electron diffraction (SAED) patterns were observed using a transmission electron microscope (JEOL JEM 2100F) at an accelerating voltage of 200 kV. Microhardness test, XRD analysis and TEM observation for the HPTed specimen were conducted in

the regions at a distance of 3.5 mm from the center of the original 10 mmφ disks in order to avoid unsaturated levels of hardness, and thus undeveloped substructures being investigated [5].

Needle-shaped samples for APT were prepared by a standard two-stage electropolishing method; i.e., a double layer technique with 25 vol% perchloric acid in acetic acid at 15 V and micro-polishing with 2 vol% perchloric acid in 2-butoxyethanol [20]. APT was carried out at a specimen temperature of 20 K with a pulse fraction (pulse voltage/steady-state voltage) of 15−20% by an atom probe instrument (CAMECA Instruments LEAP 3000HR) for the undeformed specimen (Unfortunately, no successful analysis has been accomplished for the HPTed specimen because of frequent failure of needle-shaped samples due to the ultrafine-grained structures). Visualization and quantitative estimation of the obtained three-dimensional atom-by-atom data were performed with software packages (AMETEK IVAS3.6.0 and Oxford nanoScience PoSAP) through several analyzing methods including iso-concentration surface, composition profile, autocorrelation function and frequency distribution analyses [20].

3. Results

Fig. 1 shows age-hardening curves of the undeformed and HPTed specimens at 343 K. From the values of "before aging" hardness, it is obvious that application of HPT significantly strengthens the undeformed specimen from HV120 to HV270. Such a remarkable strengthening can be explained by ultrafine-grained hardening because the corresponding TEM microstructure of the HPTed specimen before aging consists of submicrometer-scale grains (average grain size of ~100 nm) with high-angle grain boundaries (See the dark-field image and the SAED pattern in Fig. 2).

In the subsequent stage of aging, further strengthening can be achieved by prolonged aging treatment not only in the undeformed specimen but also in the HPTed specimen. The age-hardenability of ΔHV31 ± 2 for the HPTed specimen is almost identical to that of ΔHV33 ± 2 for the undeformed specimen, suggesting that concurrent strengthening by HPT and aging treatment is activated without diminishing the age-hardenability of this alloy system. It should be also emphasized that the attained hardness of the HPTed specimen reaches ~ HV296 after 2576 ks, comparable to > HV290 of our previously reported 2091Al-Li-Cu alloy subject to HPT and low-temperature aging [6,9].
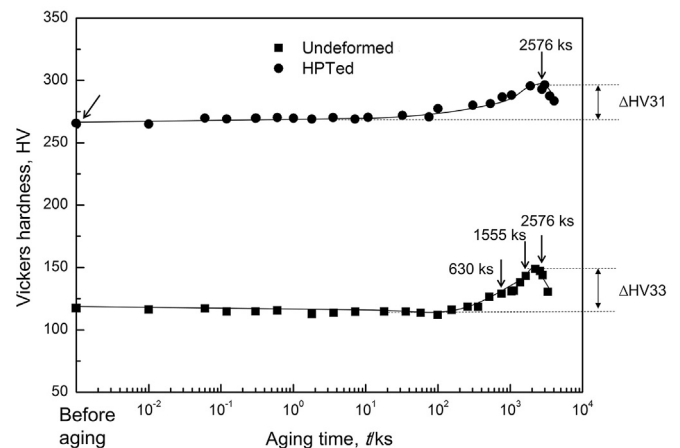

Fig. 1. Vickers hardness change of the undeformed and HPTed specimens during aging at 343 K. The conditions of aging treatment applied to the specimens for TEM and APT experiments are indicated by arrows.
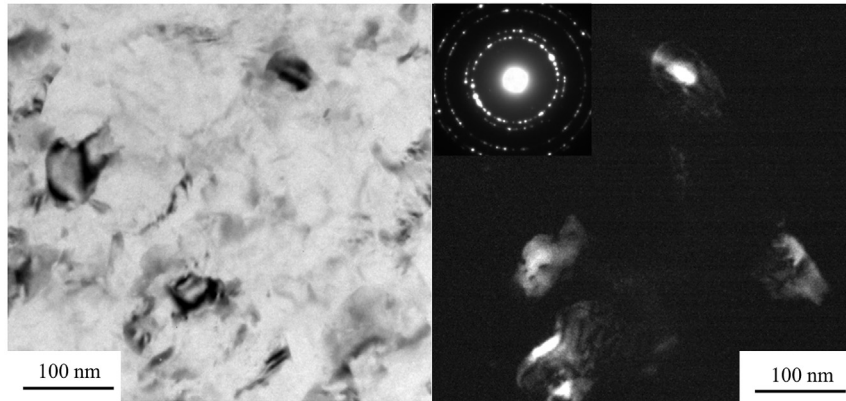
Fig. 2. Bright-field and dark-field TEM images with the corresponding SAED pattern for the HPTed specimen before aging.

Fig. 3 shows bright-field TEM images and the corresponding SAED patterns of the undeformed specimen aged at 343 K for 1555 and 2576 ks. In the earlier stage of aging, patchy pattern of phase-modulated contrast can be observed within the matrix of coarse grains (See the magnified microstructure in Fig. 3(a)). Such a modulated structure is typical of spinodally decomposed Al-Mg alloys, and thus the compositional fluctuation of Mg is expected to grow into GP zones eventually with the $L1_2$ ordered structure [13,14,16]. Fig. 3(b) confirms this phase decomposition sequence because spherical GP zones with Ashby-Brown contrast are uniformly developed after 2576ks aging with extra diffraction spots of superlattice reflections as shown by the arrow.

Similar modulated structures can be observed in the HPTed specimen. Fig. 4 shows bright-field TEM images and the

corresponding SAED pattern of the HPTed specimen aged at 343 K for 2576 ks. While average grain size of ultrafine grains remains at ~120 nm (i.e. sluggish growth from ~100 nm in Fig. 2 even after the prolonged aging treatment), it is clearly seen that phase-modulated contrast arising from compositional fluctuations is similarly present within the ultrafine grains. It is also obvious from Fig. 4 that no grain boundary precipitates with less significant role in strengthening are formed, irrespective of the ultrafine-grained structure with a high number density of grain boundaries. This finding confirms that our proposed strategy of "taking advantage of spinodal decomposition" is effective in activating concurrent strengthening by ultrafine-grained and precipitation hardenings for the investigated Al-Mg alloy.

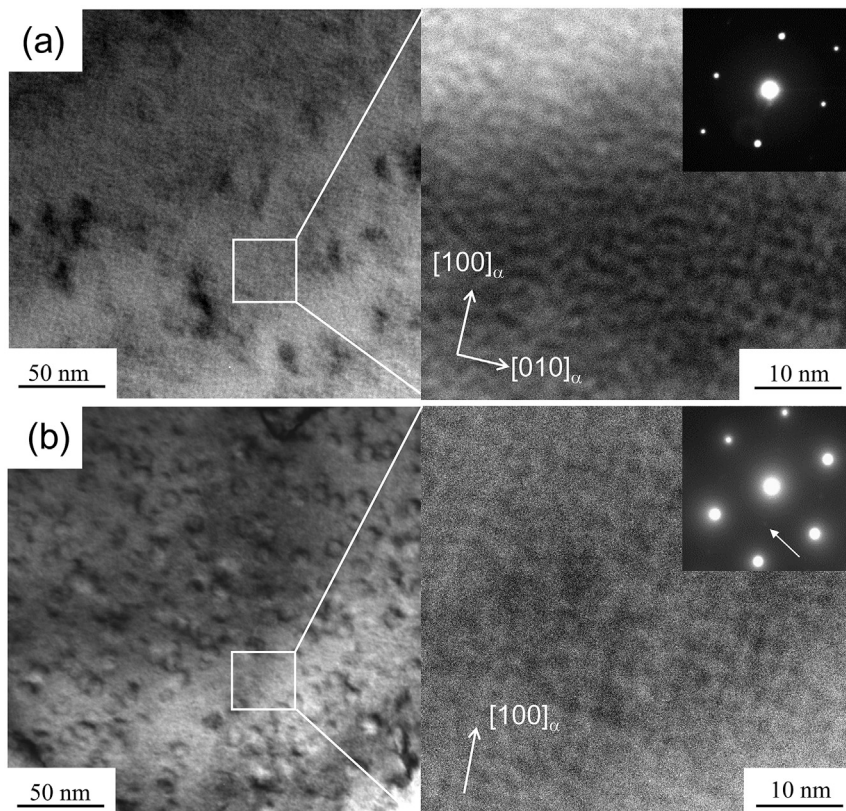In this study, APT was performed on the underformed specimen

Fig. 3. Bright-field TEM images with the corresponding SAED patterns for the undeformed specimen aged at 343 K for 1555 (a) or 2576 ks (b).
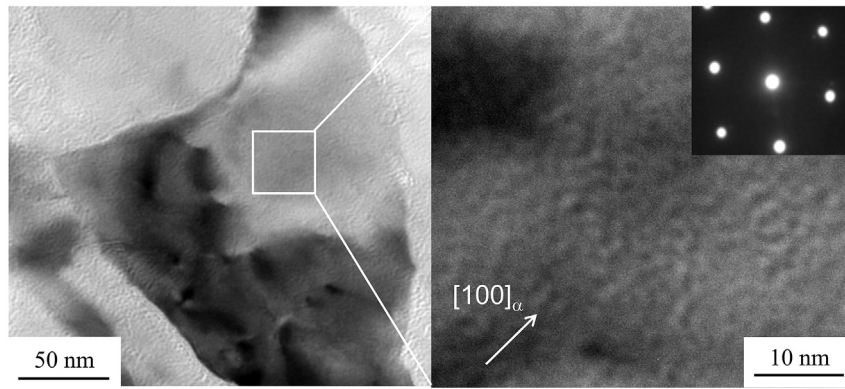
Fig. 4. Bright-field TEM images with the corresponding SAED pattern for the HPTed specimen aged at 343 K for 2576 ks.

to investigate when and how Mg concentration fluctuates in three dimensions. Fig. 5(a) and 6(a) illustrate elemental map of Mg atoms in the analyzed volume of the undeformed specimen aged at 343 K for 630 and 1555 ks. Although only Mg atoms were depicted as green points with detected overall concentration of 13.1 at% or 14.6 at%, the excess overlap of Mg atoms visually restricts the determination of the features of those microstructures. Therefore, isoconcentration map at specific isosurface levels of Mg was constructed to reveal the inhomogeneity of Mg distributions. From the comparison of white-colored isoconcentration surfaces between Figs. 5(b) and 6(b), it is obvious that compositional fluctuations develop to a great extent with increasing aging time.

To quantify the compositional fluctuations, one-dimensional composition profile along the elastically soft $[001]_\alpha$ direction of selected boxes (e.g. rectangular parallelepiped in Figs. 5(b) and 6(b)) has been drawn by taking into account crystallographic orientation of the analyzed volume through Figs. 5(c) and 6(c) (Note that perfect match of stereographic projection of $(111)_\alpha$ or $(001)_\alpha$ with detection event histogram of Mg atoms on the X-Y plane allows X, Y and Z axes of the analyzed volume to be determined, and thus the longitudinal direction of the selected boxes can be aligned to the $[001]_\alpha$ direction precisely). From the values and positions of maximum or minimum Mg concentrations on the auxiliary curves, it can be quantified that a fluctuation of Mg concentration develops from 2.4 ± 0.5 at%Mg (630ks aging) to 5.2 ± 0.7 at%Mg (1555ks aging) in amplitude with a wavelength of

~11 nm (Here, the amplitude is expressed as the average with a 2σ error, whereas the wavelength as divided Z distance by the number of wavelengths traversing the volume in Figs. 5(d) and 6(d)). Remember that no GP zones have been formed yet in the two aging conditions, as suggested by the corresponding TEM microstructures (e.g. Fig. 3(a) for 1555ks aging), because the maximum Mg concentration on the auxiliary curves does not reach the metastable equilibrium of 25 at%Mg.

4. Discussion

4.1. Quantitative estimation of modulated structures

As described in 1. Introduction, spinodal decomposition of highly concentrated Al-Mg alloys has been characterized only by TEM [13—16] or SANS [17], and thus our APT can provide new and unique information about the compositional fluctuations even though only the undeformed specimen was investigated (To authors' knowledge, ATP has been only applied to the evaluation of spinodal microstructures in iron-, copper- and titanium-based alloys [21—25], although the spatial distribution of the $\delta'-Al_3Li$ phase was depicted by the authors' APT, as evidence of spinodal decomposition (followed after congruent ordering) occurring in an Al-Li-Cu alloy [26]). For example, the above estimate of amplitude and wavelength of Mg fluctuations (i.e. 2.4 ± 0.5 at%Mg or 5.2 ± 0.7 at% Mg and ~11 nm) is based on intuitive real-space morphology of
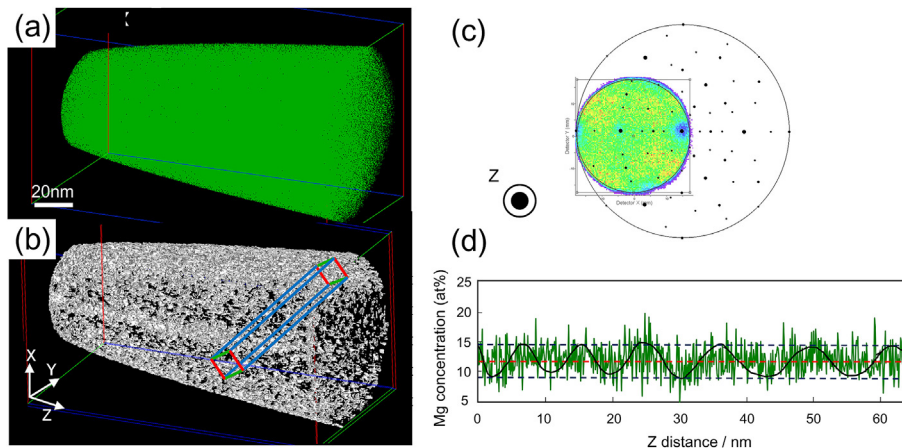

Fig. 5. Results of APT for the undeformed specimen aged at 343 K for 630 ks. (a) Elemental map of Mg atoms, (b) Isoconcentration map at isosurface level of 17.5 at%Mg (Five-point weighted smooth and grid spacing of 0.8 nm), (c) Detection event histogram of Mg atoms on the X-Y plane matched with stereographic projection of $(111)_\alpha$, (d) Composition profile of Mg along the $[001]_\alpha$ direction of the selected box in (b).
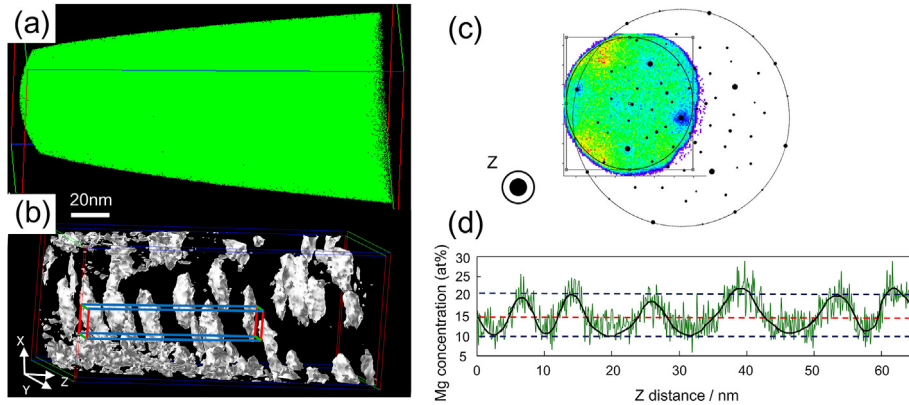
Fig. 6. Results of APT for the undeformed specimen aged at 343 K for 1555 ks. (a) Elemental map of Mg atoms, (b) Isoconcentration map at isosurface level of 18.0 at%Mg (Five-point weighted smooth and grid spacing of 0.8 nm), (c) Detection event histogram of Mg atoms on the X-Y plane matched with stereographic projection of $(001)_\alpha$, (d) Composition profile of Mg along the $[001]_\alpha$ direction of the selected box in (b).

spinodal microstructures in Figs. 5 and 6, and thus there is no need to worry about overlapping of multi-wavelength developing toward different directions, unlike in the case of transmission imaging technique such as TEM. As for the statistical reliability of the estimate, furthermore, the following two analyzing methods; i.e. autocorrelation function and frequency distribution analyses, can compensate for such a drawback of APT, as with the case of reciprocal space technique by SANS.

Fig. 7(a, c) shows one-dimensional autocorrelation function R(k) calculated from composition profiles of Mg in the undeformed specimen aged at 343 K for 630 and 1555 ks (e.g. Figs. 5(d) and 6(d)). Under this analyzing method, a positive value of R(k) is generated at lag k if a modulated two-phase microstructure is formed with a wavelength corresponding to k, whereas random solid solutions yield values of R(k) close to zero [21]. It is clearly

seen in Fig. 7(a,c) that the first positive maximum of R(k) appears at k = 12.1 ± 0.1 or 12.8 ± 0.1, and thus wavelength of those fluctuations is found to increase from 12.1 ± 0.1 nm to 12.8 ± 0.1 nm during the period from 630ks to 1555 ks (Thus, a minor adjustment of the manually estimated wavelength of ~11 nm has to be made). Similar value of 12.5 nm is reported for an Al-10 wt%Mg alloy naturally aged for 1980 ks, in which not only the periodicity of phase-modulated contrast along the $[001]_\alpha$ direction but also the diffuse appearance of satellite spots (or sidebands) near each Bragg reflection was carefully investigated on the SAED patterns [13,14] (N.B. Such satellite spots are characteristic of periodic modulations of composition, and from those spacing the wavelength of the modulation can be determined as average quantity through the Daniel-Lipson equation [27]).

As for the amplitude of compositional fluctuations, on the other
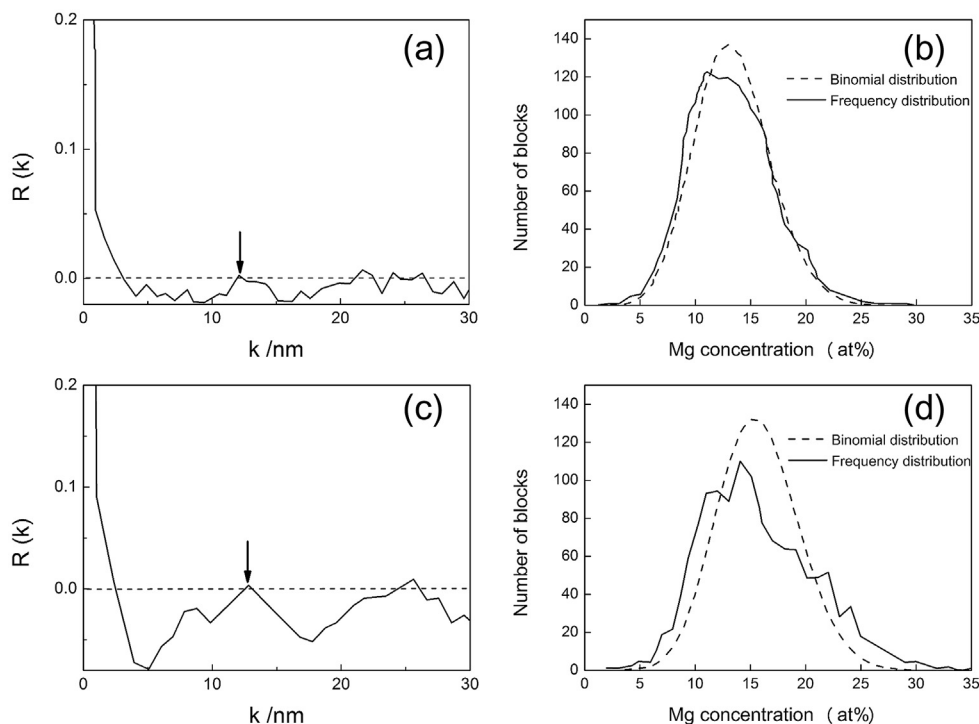
Fig. 7. (a, c) One-dimensional autocorrelation function calculated from the composition profiles of Mg in Figs. 5(d) and 6(d) and (b, d) frequency distribution curve of Mg concentrations estimated from overall APT data in Figs. 5(a) and 6(a) for the undeformed specimen aged at 343 K for 630 (a, b) and 1555 ks (c, d).

hand, neither TEM nor SANS could estimate quantitatively. Fig. 7(b,d) shows frequency distribution curves of Mg concentrations, constructed by dividing overall APT data (e.g. Figs. 5(a) and 6(a)) into equal sized blocks of 100 atoms and plotting the observed number of blocks with each composition, for the undeformed specimen aged at 343 K for 630 and 1555 ks. Slight deviation of frequency distribution from binomial distribution (corresponding to random solid solution) can be seen after 630ks aging, and then a further broadening of the frequency distribution is found to occur after 1555ks aging. The corresponding χ^2 test also proved such an inhomogeneity of Mg distributions because the null hypothesis of random solid solution was rejected with >99.9% of significance level. This finding provides collateral evidence of the development of spinodal decomposition, and prolonged aging treatment is expected to yield the frequency distribution with more than one peak corresponding to the decomposed Mg-rich and Mg-lean regions [20].

4.2. Strengthening by spinodal decomposition

It is known that spinodal decomposition can enhance the mechanical properties of iron-, copper-, titanium-, aluminum-, manganese-based and other alloys [14,28–33], and the hardening mechanism (i.e. spinodal-hardening mechanism) has been proposed by several researches [34–38] including Cahn, who established the present spinodal decomposition theory [39,40]. After taking those proposed mechanisms into consideration, Kato et al. [18] conclusively demonstrated based on a force balance equation of mixed dislocations that the increment in yield stress caused by coherent internal stress in a fcc alloy is proportional to the amplitude of compositional fluctuation, but independent of wavelength, of the modulated structures;

$$\Delta\sigma = \frac{A|\eta|Y}{\sqrt{6}}, \tag{1}$$

where $\Delta\sigma$ is the increment in yield stress [$= M\Delta\tau_{CRSS}$], M is Taylor factor (= 3.06 for fcc metals), $\Delta\tau_{CRSS}$ is the increment in critical resolved shear stress, A is the amplitude of the compositional fluctuation, η is lattice mismatch [$=(1/a)\,(\partial a/\partial c)$], $\partial a/\partial c$ is the composition variation of stress-free lattice parameter a with respect to Mg concentration c, and Y is elastic modulus calculated from elastic constants C. In the case of aluminum with fcc structure, the values of

$$
\begin{aligned}
Y_{\langle 100\rangle} &= (C_{11} + 2C_{12})\,(C_{11} - C_{12})/C_{11} \\
Y_{\langle 110\rangle} &= (C_{11} + 2C_{12})(C_{11} + 6C_{44} - C_{12})/[2(C_{11} + 2C_{44} + C_{12})\,] \\
Y_{\langle 111\rangle} &= 6(C_{11} + 2C_{12})C_{44}/(4C_{44} + C_{11} + 2C_{12})
\end{aligned}
\tag{2}
$$

are estimated as 98.7, 110 and 114 GPa, respectively, from $C_{11} = 107$, $C_{12} = 60.8$ and $C_{44} = 28.3$ GPa [40], and thus the modulated structures are confirmed to develop along the elastically soft $[001]_\alpha$ direction, as observed in composition profiles of Mg in Figs. 5(d) and 6(d). Assuming that Vickers hardness is proportional to yield stress with a proportionality constant of ~3 [41], therefore, the increment of Vickers hardness can be correlated to the amplitude A through

$$\Delta HV \propto \frac{A|\eta|Y}{\sqrt{6}}. \tag{3}$$

Fig. 8 shows the relationship between the increment of Vickers hardness (i.e. $\Delta HV = 13.5 \pm 2$ and $\Delta HV = 25 \pm 2$ in Fig. 1) and the estimated amplitude of Mg fluctuations (i.e. $A = 2.4 \pm 0.5$ at%Mg and $A = 5.2 \pm 0.7$ at%Mg in Figs. 5(d) and 6(d)) for the undeformed
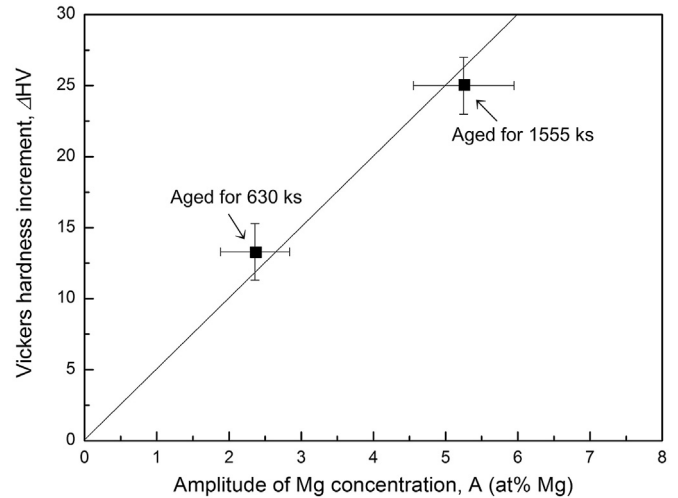

Fig. 8. Relationship between the increment of Vickers hardness (Fig. 1) and the estimated amplitude of Mg fluctuations (Figs. 5(d) and 6(d)) during aging of the undeformed specimen at 343 K.

specimen aged at 343 K for 630 and 1555 ks. From the good linearity through the two plots, it can be deduced that the development of coherent internal stress associated with modulated structures is attributed to the strengthening by spinodal decomposition as predicted by Kato et al. [18]. Note that the coherent internal stress is originated from the difference of atomic radii between Al and Mg, and thus with increasing amplitude dislocation movement during deformation is hindered.

The same spinodal-hardening mechanism is considered to activate in the HPTed specimen with a high number density of grain boundaries. As described in 3. Results, the age-hardenability of $\Delta HV 31 \pm 2$ for the HPTed specimen was almost identical to that of $\Delta HV 33 \pm 2$ for the undeformed specimen (Fig. 1), and modulated structure was similarly observed within the ultrafine grains in the HPTed specimen without grain boundary precipitates (Fig. 4). It is no surprise, therefore, that spinodal decomposition is supposed to proceed even in the HPTed specimen because the wavelength of 12.1 ± 0.1 nm or 12.8 ± 0.1 nm (Fig. 7(a,c)) is sufficiently smaller than the average grain size of ~100 nm or ~120 nm (Figs. 2 and 4). The sluggish growth of the ultrafine grains even after 2576ks aging also maintains the contribution of ultrafine-grained hardening, but unfortunately SPD induced GB segregation of Mg atoms [42] failed to be detected in this study, leaving the reason why the ultrafine grains grow so sluggishly as a subject of further investigation.

4.3. Influence of severe plastic deformation on spinodal decomposition

It is well known that ultrafine-grained structures contain a high density of defects such as dislocations and vacancies, and might affect the mobility of solute atoms and thus at least the kinetics of phase decomposition [43]. The application of HPT can achieve supersaturated solid solutions of excess amount of alloying elements [44], and in fact both the undeformed and HPTed specimens possessed the super-saturated solid solutions in the "before aging" condition, as suggested by the absence of any reflections from Mg or other compounds in the obtained (but unshown) XRD profiles. Fig. 9 shows determination procedure of lattice parameters of the super-saturated solid solutions from their XRD profiles through Cohen's least-squares method [45,46]. Almost equivalent lattice parameters of 0.4101 and 0.4106 nm were estimated from
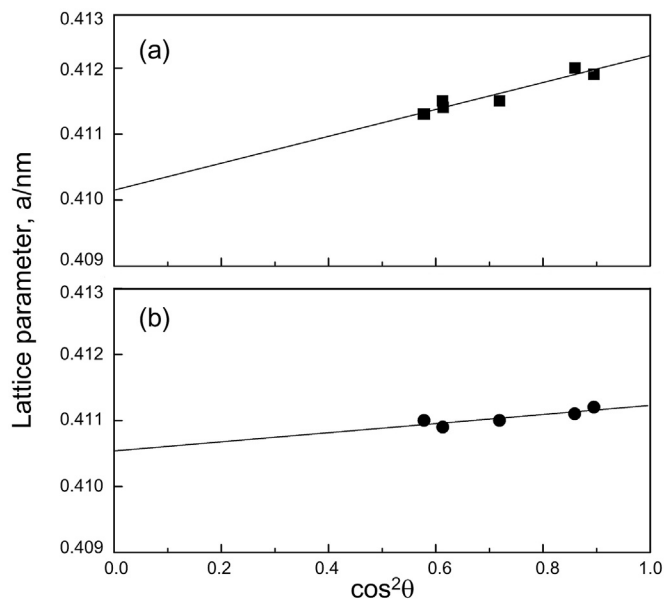
Fig. 9. Determination procedure of lattice parameters of the obtained super-saturated solid solutions from XRD profiles for the (a) undeformed and (b) HPTed specimens through Cohen's least-squares method [45,46].

intersections of extrapolation lines through plots of a ($=(h^2+k^2+l^2)^{1/2}d$) vs $\cos^2\theta$ (Here, h, k, l are Miller indices of a Bragg plane, and d is the lattice spacing calculated from $\lambda/2\sin\theta$), in agreement with reported lattice parameters of supersaturated Al-(5−40)wt%Mg alloy subject to HPT [44]. Such an equivalent lattice parameter, and thus equivalent Mg concentration in the matrix, leads to the equal contribution of solid-solution hardening by Mg atoms for both the undeformed and HPTed specimens. Therefore, remarkable increase in "before aging" hardness in Fig. 1 can be explained by SPD induced ultrafine-grained hardening alone.

In the subsequent stage of aging, furthermore, the effect of ultrafine-grained structures on spinodal decomposition might be involved in Fig. 1, but unfortunately the softening by the growth of ultrafine grains (i.e. from ~100 nm in Fig. 2 to ~120 nm in Fig. 4) makes it impossible to evaluate the degree and kinetics of spinodal decomposition in the HPTed specimen precisely. The quantification of Mg fluctuations in the fragile HPTed specimen is in progress by laser-assisted APT.

4.4. Concurrent strengthening of ultrafine-grained age-hardenable aluminum alloy

One of the significant achievements in this study was to fabricate again novel Al-Mg alloy with a higher attained hardness (i.e. ~HV296) by means of concurrent strengthening by ultrafine-grained and precipitation hardenings. Following the success of our previously reported 2091Al-Li-Cu alloy [6,9], it was verified that the HPTed specimen of the Al-13.4 wt%Mg model alloy can be also strengthened by aging treatment at a lower temperature. Although there are still problems to be solved, e.g. poor ductility and poor corrosion resistance of such a highly concentrated Al-Mg alloy, the effectiveness of our proposed strategy to achieve concurrent strengthening; i.e. "taking advantage of spinodal decomposition", was proved to be applicable to the alloys that decompose via spinodal decomposition. In contrast, in the case of the alloys that decompose via nucleation and growth process, the other two strategies; i.e. lowering of aging temperature (within miscibility gap, but above spinodal lines) and utilization of microalloying

elements [47−50], are effective in maximizing the effect of concurrent strengthening by ultrafine-grained and precipitation hardenings, as previously reported for Al-Mg-Si(-Cu) alloys in Refs. [6,9]. Therefore, our proposed three strategies are useful for designing any concurrently strengthened severely-deformed age-hardenable aluminum alloys.

5. Conclusions

In this study, concurrent strengthening of ultrafine-grained age-hardenable Al-13.4 wt%Mg (Al-14.7 at%Mg) alloy has been successfully accomplished by combined processing of HPT and aging treatment at 343 K below the spinodal line. Not only a higher attained hardness of >HV 296 was obtained, but also the good age-hardenability of ΔHV31 $\pm$ 2 was maintained almost comparable to that of ΔHV33 $\pm$ 2 for the undeformed specimen without HPT. The corresponding TEM images exhibited patchy pattern of phase-modulated contrast typical of spinodally decomposed microstructures, and APT could detect and quantify the fluctuation of Mg concentrations developing along the $[001]_\alpha$ direction. The amplitude of Mg fluctuations in the undeformed specimen was found to increase from 2.4 $\pm$ 0.5 at%Mg to 5.2 $\pm$ 0.7 at%Mg during aging from 630ks to 1555ks with wavelengths of 12.1 $\pm$ 0.1 nm and 12.8 $\pm$ 0.1 nm, and the good linearity between the increment in hardness and the estimated amplitude strongly supported Kato's spinodal-hardening mechanism. By taking into account the fact that the wavelength is sufficiently smaller than average size of ultrafine grains (i.e. ~100 nm or ~120 nm), spinodal decomposition is supposed to proceed even in the HPTed specimen. Therefore, the effectiveness of our proposed strategy to achieve concurrent strengthening; i.e. "taking advantage of spinodal decomposition", is verified for the alloys that decompose via spinodal decomposition.

References

[1] W.J. Kim, C.S. Chung, D.S. Ma, S.I. Hong, H.K. Kim, Optimization of strength and ductility of 2024 Al by equal channel angular pressing (ECAP) and post-ECAP aging, Scr. Mater. 49 (2003) 333–338.
[2] Z. Horita, K. Ohashi, T. Fujita, K. Kaneko, T.G. Langdon, Achieving high strength and high ductility in precipitation-hardened alloys, Adv. Mater. 17 (2005) 1599–1602.
[3] Y.H. Zhao, X.Z. Liao, S. Cheng, E. Ma, Y.T. Zhu, Simultaneously increasing the ductility and strength of nanostructured alloys, Adv. Mater. 18 (2006) 2280–2283.
[4] K. Ohashi, T. Fujita, K. Kaneko, Z. Horita, T.G. Langdon, The aging characteristics of an Al−Ag alloy processed by equal-channel angular pressing, Mater. Sci. Eng. A 437 (2006) 240–247.
[5] S. Lee, Z. Horita, S. Hirosawa, K. Matsuda, Age-hardening of an Al−Li−Cu−Mg alloy (2091) processed by high-pressure torsion, Mater. Sci. Eng. A 546 (2012) 82–89.
[6] S. Hirosawa, T. Hamaoka, Z. Horita, S. Lee, K. Matsuda, D. Terada, Methods for designing concurrently strengthened severely deformed age-hardenable aluminum alloys by ultrafine-grained and precipitation hardenings, Met. Mater. Trans. A 44 (2013) 3921–3933.
[7] A. Deschamps, F. De Geuser, Z. Horita, S. Lee, G. Renou, Precipitation kinetics in a severely plastically deformed 7075 aluminium alloy, Acta Mater. 66 (2014) 105–117.

[8] I.F. Mohamed, S. Lee, K. Edalati, Z. Horita, S. Hirosawa, K. Matsuda, D. Terada, Aging behavior of Al 6061 alloy processed by high-pressure torsion and subsequent aging, Metall. Mater. Trans. A 46 (2015) 2664–2673.

[9] S. Hirosawa, Y. Tang, Z. Horita, S. Lee, K. Matsuda, D. Terada, Three strategies to achieve concurrent strengthening by ultrafine-grained and precipitation hardenings for severely deformed age-hardenable aluminum alloys, Adv. Mater. Res. 1135 (2016) 161–166.

[10] A. Azushima, R. Kopp, A. Korhonen, D.Y. Yang, F. Micari, G.D. Lahoti, P. Groche, J. Yanagimoto, N. Tsuji, A. Rosochowski, A. Yanagida, Severe plastic deformation (SPD) processes for metals, CIRP Ann. Manuf. Technol. 57 (2008) 716–735.

[11] J. Gubicza, I. Schiller, N.Q. Chinh, J. Illy, Z. Horita, T.G. Langdon, The effect of severe plastic deformation on precipitation in supersaturated Al–Zn–Mg alloys, Mater. Sci. Eng. A 460–461 (2007) 77–85.

[12] M.J. Starink, A.M. Zahra, Low temperature decomposition of Al-Mg alloys: GP zones and L1$_2$ ordered precipitates, Philos. Mag. A 76 (1997) 701–714.

[13] T. Sato, A. Kamio, High resolution electron microscopy of phase decomposition microstructures in aluminium-based alloys, Mater. Sci. Eng. A 146 (1991) 161–180.

[14] T. Sato, Y. Kojima, T. Takahashi, Modulated structures and GP zones in Al-Mg alloys, Metall. Trans. A 13 (1982) 1373–1378.

[15] E.K. Boudili, M.F. Denanot, A. Dauger, Decomposition of supersaturated solid solutions of Al-Mg at 20°C, Scr. Metall. 11 (1977) 543–548.

[16] C. Gault, A. Dauger, P. Boch, Decomposition of aluminium-magnesium solid solutions studied by ultrasonic measurements of elastic properties and electron microscopy, Acta Metall. 28 (1980) 51–60.

[17] A. Dauger, M. Fumeron, J.P. Guillot, M. Roth, Small-angle neutron scattering of single crystals of aged aluminium-13 at% magnesium alloy, J. Appl. Cryst. 12 (1979) 429–431.

[18] M. Kato, T. Mori, I.H. Schwartz, Hardening by spinodal modulated structure, Acta Metall. 28 (1980) 285–290.

[19] H.W.L. Phillips, The constitution of alloys of aluminium with magnesium, silicon and iron, J. Inst. Met. 72 (1946) 151–227.

[20] M.K. Miller, Atom Probe Tomography, Kluwer Academic, New York, 2000, p. 174.

[21] M.K. Miller, J.M. Hyde, M.G. Heterington, A. Cerezo, G.D.W. Smith, C.M. Elliott, Spinodal decomposition in Fe-Cr alloys: experimental study at the atomic level and comparison with computer models—I. Introduction and methodology, Acta Metal. Mater. 43 (1995) 3385–3401.

[22] F. Danoix, P. Auger, Atom probe studies of the Fe–Cr system and stainless steels aged at intermediate temperature: a review, Mater. Charact. 44 (2000) 177–201.

[23] J. Zhou, J. Odqvist, M. Thuvander, P. Hedström, Quantitative evaluation of spinodal decomposition in Fe-Cr by atom probe tomography and radial distribution function analysis, Microsc. Microanal. 19 (2013) 665–675.

[24] C.M. Müller, A.S. Sologubenko, S.S.A. Gerstl, R. Spolenak, On spinodal decomposition in Cu–34at%Ta thin films – an atom probe tomography and transmission electron microscopy study, Acta Mater. 89 (2015) 181–192.

[25] L.J.S. Johnson, M. Thuvander, K. Stiller, M. Odén, L. Hultman, Spinodal decomposition of Ti$_{0.33}$Al$_{0.67}$N thin films studied by atom probe tomography, Thin Solid Films 520 (2012) 4362–4368.

[26] S. Hirosawa, Y. Tang, Z. Horita, K. Matsuda, S. Lee, D. Terada, Development of novel wrought aluminum alloys concurrently strengthened by ultrafine-grained and precipitation hardenings, J. Jpn. Soc. Heat Treat. (Netsu-shori) 55 (2015) 307–308.

[27] V. Daniel, H. Lipson, An X-ray study of the dissociation of an alloy of copper, iron and nickel, Proc. Roy. Soc. A 181 (1943) 368–378.

[28] K.H. Park, J.C. Lasalle, L.H. Schwartz, M. Kato, Mechanical properties of spinodally decomposed Fe-30wt% Cr alloys: yield strength and aging embrittlement, Acta Metall. 34 (1986) 1853–1865.

[29] M. Doi, H. Tanabe, T. Miyazaki, Development of ultra high strength steels based on spinodal decomposition, J. Mater. Sci. 22 (1987) 1328–1334.

[30] E.P. Butler, G. Thomas, Structure and properties of spinodally decomposed Cu-Ni-Fe alloys, Acta Metall. 18 (1970) 347–365.

[31] T. Miyazaki, E. Yajima, H. Suga, Influence of structural modulation on the yield stress of copper-5 at% Titanium alloy, Trans. Jpn. Inst. Met. 12 (1971) 119–124.

[32] F. Findik, Improvements in spinodal alloys from past to present, Mater. Des. 42 (2012) 131–146.

[33] J. Yan, N. Li, X. Fu, Y. Zhang, The strengthening effect of spinodal decomposition and twinning structure in MnCu-based alloy, Mater. Sci. Eng. A 618 (2014) 205–209.

[34] J.W. Cahn, Hardening by spinodal decomposition, Acta Metall. 11 (1963) 1275–1282.

[35] S.D. Dahlgren, Ph.D Thesis, Univ. of California, Berkeley, CA, USA, 1966.

[36] B. Ditchek, L.H. Schwartz, On the strength of spinodal alloys, in: Proc. 4th Inter. Conf. on Strength of Metals and Alloys, vol. 3, 1976, p. 1319.

[37] Y. Hanai, T. Miyazaki, H. Mori, Theoretical estimation of the effect of interfacial energy on the mechanical strength of spinodally decomposed alloys, J. Mater. Sci. 14 (1979) 599–606.

[38] D.N. Ghista, W.D. Nix, A dislocation model pertaining to the strength of elastically inhomogeneous materials, Mater. Sci. Eng. 3 (1969) 293–298.

[39] J.W. Cahn, On spinodal decomposition, Acta Metall. 9 (1961) 795–801.

[40] J.W. Cahn, On spinodal decomposition in cubic crystals, Acta Metall. 10 (1962) 179–183.

[41] D. Tabor, The physical meaning of indentation and scratch hardness, Br. J. Appl. Phys. 7 (1956) 159–166.

[42] X. Sauvage, N. Enikeev, R. Valiev, Y. Nasedkina, M. Murashkin, Acta Mater. 72 (2014) 125–136.

[43] R. Würschum, B. Oberdorfer, E. Steyskal, W. Sprengel, W. Puff, P. Pikart, C. Hugenschmidt, R. Pippan, Free volumes in bulk nanocrystalline metals studied by the complementary techniques of positron annihilation and dilatometry, Phys. B 407 (2012) 2670–2675.

[44] K. Kaneko, T. Hata, T. Tokunaga, Z. Horita, Fabrication and characterization of supersaturated Al-Mg alloys by severe plastic deformation and their mechanical properties, Mater. Trans. 50 (2009) 76–81.

[45] M.U. Cohen, Precision lattice constants from X-ray powder photographs, Rev. Sci. Instrum. 6 (1935) 68–74.

[46] M.U. Cohen, Precision lattice constants from X-ray powder photographs, Rev. Sci. Instrum. 7 (1936), 155–155.

[47] T. Sato, S. Hirosawa, K. Hirose, T. Maeguchi, Roles of microalloying elements on the cluster formation in the initial stage of phase decomposition of Al-based alloys, Met. Mater. Trans. A 34 (2003) 2745–2755.

[48] S. Hirosawa, T. Omura, Y. Suzuki, T. Sato, Improvement of bake-hardening response of Al-Mg-Cu alloys by means of nanocluster assist processing (NCAP) technique, Mater. Sci. Forum 519–521 (2006) 215–220.

[49] S. Hirosawa, F. Nakamura, T. Sato, First-principles calculation of interaction energies between solutes and/or vacancies for predicting atomistic behaviors of microalloying elements in aluminum alloys, Mater. Sci. Forum 561–565 (2007) 283–286.

[50] Y. Koshino, M. Kozuka, S. Hirosawa, Y. Aruga, Comparative and complementary characterization of precipitate microstructures in Al-Mg-Si(-Li) alloys by transmission electron microscopy, energy dispersive X-ray spectroscopy and atom probe tomography, J. Alloys Compd. 622 (2015) 765–770.